

1 Introduction

Among the key observational properties of main sequence stars in our Galaxy, age is the most difficult to determine. Traditionally, fitting isochrones to cluster stars was one of the only precise methods for measuring ages but was extremely difficult for the majority of isolated field stars, particularly for those without precise spectroscopic information. Methods such as asteroseismology and measuring Lithium abundances can provide precise ages but require time intensive observations for each target and are not capable of producing the large quantity of ages needed for exoplanet and galactic population studies. To improve our understanding of star and planet formation and evolution, as well as the history of the Milky Way, we must constrain the ages of low-mass stars like the Sun in the galactic field.

Fortunately nature has provided a powerful means to determine ages for main sequence stars via their rotation. Angular momentum is carried away through magnetically driven stellar winds, which slows the star's rotation over cosmic time. This rotation-based "clock" is known as *gyrochronology*. Cool spots on the star's surface rotate in-to and out-of view, creating small amplitude ($\sim 1\%$) quasi-periodic changes in the stellar brightness. While rotation periods have previously been measured from starspot-induced flux modulations for hundreds of stars from the ground, space-based photometric surveys have opened the door to homogeneous ensemble measures of stellar rotation, and therefore age. **With precise, long-duration light curves available from the *Kepler*/K2 mission, we can determine rotation periods and ages for nearly 100,000 main sequence field stars.**

The *Kepler* mission broke new ground by producing rotation periods for over 34,000 field stars within a single ~ 110 sq deg field of view, and discovered a surprising bimodal distribution of rotation periods (McQuillan et al., 2014). Two competing explanations have arisen for this mysterious feature: a bimodal age distribution for nearby stars, or a new subtlety in stellar angular-momentum-loss mechanisms. Detailed calibrations of gyrochronology models with the *Kepler* rotation sample also revealed the need for samples of stars with a wider range of ages and compositions. Fortunately the ongoing *Kepler* extended mission, K2, has currently produced light curves from 14 additional fields throughout the Galaxy.

To enable studies of stellar ages from rotation periods with K2, we propose to:

1. Measure accurate rotation periods for every available K2 target, using the most appropriate tools and methods required. This value-added dataset will improve the *Kepler* data legacy for field stars, and provide a critical training set for the TESS mission.
2. Produce updated gyrochronology relations based on a wider range of field star ages, and additional open clusters within the K2 fields.
3. Determine the origin of the mysterious rotation period bimodality discovered with *Kepler* by tracing the rotation period distribution in each K2 field, and out to further distances utilizing public Gaia data.
4. Measure the star formation history within each K2 field using a new Bayesian age-dating system.

2 Scientific Motivation

Galactic archaeology and exoplanet populations are two rapidly accelerating fields of interest within astronomy. Although seemingly unconnected, these two fields are linked by a mutual requirement for precise stellar parameters. To galactic archaeologists, ages and elemental abundances are the most important parameters. Indeed, most galactic archaeology surveys target exactly these properties. For exoplaneteers, masses and radii have historically been the most important stellar parameters for understanding planetary systems. With a growing number of planet hosts with precise masses and radii, attention is turning toward other parameters such as ages to understand the history and evolution of these systems. Age is therefore a fundamental stellar parameter of great interest to two large communities of astronomers. However it is a difficult attribute to measure for main sequence F, G, K, and M stars in the field, in part because low-mass dwarfs do not move far on the Color-Magnitude diagram (CMD) during their hydrogen burning lifetimes. Further, competing stellar evolution models predict different ages for the same star. Of the measurable properties for a large ensemble of field stars, rotation periods contain the most information about stellar age, and provide the best leverage for advancing our knowledge of galactic archeology as well as exoplanet population demographics.

2.1 Age-Dating Field Stars with Rotation

The seminal work of Skumanich (1972) laid the foundation for our model of the stellar age–rotation–activity relationship. When stars settle onto the main sequence they may have a range of initial rotation periods based on the angular momentum available in their primordial environment. However, rotation velocities for Solar-type stars converge after around 500 Myr (Radick et al., 1987; Irwin & Bouvier, 2009), and then follow a standard spin-down evolution (Barnes, 2010). Main sequence stars continuously lose angular momentum due to magnetically driven winds (Schatzman, 1962; Weber & Davis, 1967; Mestel, 1984; Kawaler, 1988; Charbonneau, 2010). Since stellar rotation also drives the internal magnetic dynamo (Schatzman, 1962; Parker, 1970), the result of this angular momentum loss is decreasing surface magnetic activity as the star slows. Older, slower rotating stars therefore have smaller starspots, making the detection of their rotation more difficult as stars age. This rate of angular momentum loss has a dependence on the stellar mass (Noyes et al., 1984). Deriving ages for field stars therefore requires knowing their color (as a proxy for stellar mass) and their present-day surface rotation period (Barnes, 2007).

The rate of this angular momentum loss has historically been calibrated using main sequence stars at a range of masses in stellar clusters with known ages, leading to a useful clock called “gyrochronology” (Barnes, 2003). Several gyrochronology model parameterizations exist, each using various age benchmarks for calibration (*e.g.* Barnes, 2007, 2010; Mamajek & Hillenbrand, 2008; Angus et al., 2015; Matt et al., 2012; van Saders & Pinsonneault, 2013; van Saders et al., 2016). Nearly all gyrochronology models suffer from lack of constraints at older ages; often the Sun is the only benchmark used older than ~ 1 Gyr since accessible nearby open clusters are typically young (< 600 Myr).

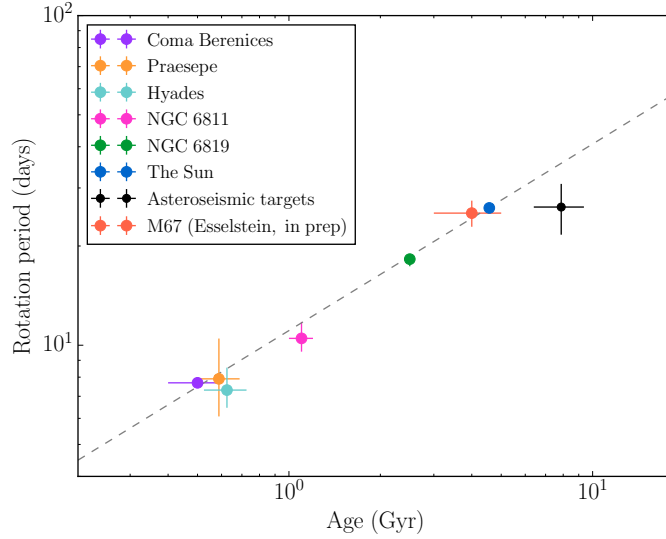


Figure 1: A gyrochronology relation (dashed grey line) demonstrating the rotational evolution of stars with precise ages. Median rotation periods for Solar-type stars in open clusters (colored points), Solar mass *Kepler* asteroseismic targets (black point), and the Sun (blue point). The black point falls below the straight line, indicating that there may be a transition in age-rotation relation at around Solar age.

In Figure 1 we demonstrate the discrepancy between a single power-law gyrochronology model and the most recent asteroseismic data from the *Kepler* sample. As first demonstrated in Angus et al. (2015), the asteroseismic stars seem to be too rapidly rotating given their age, according to the gyrochronology models. This finding was supported by van Saders et al. (2016) who used *Kepler* asteroseismic targets to redefine the gyrochronology models. To explain this phenomenon van Saders et al. (2016) invoke a transitioning magnetic dynamo behavior at a critical Rossby number, Ro^1 which they find to be $Ro \approx 2.7$ (close to the Solar value). This transition marks a boundary between efficient magnetic braking ($2.7 < Ro$) to inefficient braking ($Ro < 2.7$); stars stop spinning down after their rotation slows enough to cross this critical threshold. **This has extremely important consequences for gyrochronology: can we trust ages inferred from rotation for slowly rotating stars like the Sun?**

Additional calibration sources are desperately needed for stars older than the Sun in order to confirm these hints of a changing angular momentum loss rate due to a transitioning magnetic dynamo. Asteroseismology also cannot yet provide ages for stars with masses much lower than the Sun, leading to an incomplete calibration of the gyrochronology models. Douglas et al. (2017) used K2 observations of the Hyades to demonstrate that gyrochronology may be applicable to stars with masses as low as $0.3 M_{\odot}$. While rotation periods of many more low-mass stars are needed to confirm this exciting finding, if confirmed it would be an

¹The Rossby number is the ratio of rotation period to convective overturn time.

important result for exoplanet studies, which have increased focus on M dwarfs due to the higher signal-to-noise provided by their smaller stellar radii and masses.

2.2 Rotation Periods from *Kepler* and K2

Previous ground-based efforts to constrain stellar rotation periods for single, isolated field stars have resulted in few measurements. Detecting rotation from Doppler line broadening requires obtaining medium- to high-resolution spectroscopy of individual targets, and can be subject to systematic effects such as from stellar limb darkening approximations (Collins & Truax, 1995). These observations also require time on larger aperture telescopes to reach fainter magnitudes needed to study rotation from low-mass field stars, or for studying the entire mass range within stellar clusters. Ground-based photometric wide-field surveys overcome many of the difficulties in gather large samples of field stars or entire stellar clusters. However, long duration monitoring with relatively high cadence and high photometric precision is required to detect the small amplitude and slowly varying flux modulations from starspots. These campaigns typically yielded rotation samples of hundreds to ~ 1000 for both field stars (e.g. Hartman et al., 2011) and selected young open clusters (e.g. Agüeros et al., 2011; Douglas et al., 2014; Covey et al., 2016)

Space-based photometry surveys designed for exoplanet transit searches such as *Kepler* (Borucki et al., 2010) have produced a revolution in stellar rotation studies. The original *Kepler* mission produced light curves up to four years in duration with ~ 100 ppm precision at 30-minute cadence for more than 200,000 stars. From this remarkable dataset, more than 30,000 unique stellar rotation periods have been measured using a variety of time series analysis techniques such as the Lomb-Scargle Periodogram (Reinhold et al., 2013) and the Autocorrelation Function (McQuillan et al., 2014). This bounty of rotation periods has also allowed the first ensemble investigations into stellar surface differential rotation (e.g. Reinhold et al., 2013), revealed stars with near solid-body rotation (Davenport et al., 2015), and highlighted the many degeneracies in disentangling starspot evolution and differential rotation (Aigrain et al., 2015).

After hardware failures made observations of the original field impossible, an extended *Kepler* mission was designed to observe many fields with ~ 3 month durations. The K2 mission has observed fields spaced along the ecliptic plane, ranging from low galactic latitudes that include multiple open clusters, to high galactic latitudes that include many older field stars (Howell et al., 2014). The K2 fields also include several benchmark stellar clusters including the Solar-age M67, the Pleiades and Hyades, and M35. To date K2 has released data from 10 distinct campaigns (or fields), including more than 204,000 targets. An additional 4 campaigns are underway with $\sim 94,000$ targets announced, and 2 campaigns pending scheduling. In total, the K2 sample may yield over 350,000 light curves, far exceeding the original *Kepler* mission. Importantly, K2 data quality has been demonstrated to approach that of the original *Kepler* mission (Luger et al., 2016), and has been successfully used to measure rotation periods for select targets such as open cluster stars (e.g. Douglas et al., 2017).

K2 provides the ideal dataset to both extend the *Kepler* studies of field

star age distributions, and to amass a sample of better calibration sources for gyrochronology models. The range of K2 field positions within the Galaxy means the sample spans a much wider variety of stellar ages for more distant stars ($\gtrsim 1\text{pc}$), and provides multiple opportunities to constrain the local star formation history for nearby stars. This makes the gyrochronology study of field stars with K2 an unique and valuable comparison to complimentary efforts in studying galactic archeology using chemical abundances, such as with APOGEE (Hayden et al., 2014). Producing rotation periods for these older stars and additional open clusters available in the K2 data, including the benchmark Solar-age cluster M67, will also lead to new gyrochronology relations and to test the universality of the age–rotation–activity relation put into question by Angus et al. (2015).

2.3 A Mysterious Period Bimodality

One of the most remarkable results from the *Kepler* rotation period catalog was the discovery of a bimodal period distribution among field stars by McQuillan et al. (2013), which is shown in Figure 2a. While a separate sequence of rapid rotation periods had been known in young stellar clusters due to lower-mass stars settling on to the angular momentum main sequence slower (e.g. Barnes, 2007), this new bimodality was detected from slower rotating M dwarfs ($T_{\text{eff}} \lesssim 4000$). The bimodality separated M dwarfs into two populations, those with rotation periods longer than ~ 20 days, and those with periods between ~ 1 and 20 days. Follow-up analysis of the *Kepler* data by McQuillan et al. (2014) found the period bimodality extended to include K dwarfs. **Recently, PI Davenport discovered this period bimodality extends throughout all masses in the *Kepler* rotation sample for nearby stars, as shown in Figure 2b (Davenport, 2017).**

Two formation scenarios have been proposed to explain the observed period bimodality. The first scenario, initially proposed by McQuillan et al. (2013), is the rotation period distribution reflects the local star formation history, and thus the bimodality represents a drop in the star formation rate around 600 Myr ago. This model is supported by both the extension of the bimodality to earlier spectral types by Davenport (2017), and also the tentative detection that the two rotation period populations have distinct proper motion distributions. However, such a variation in the star formation rate on short timescales has some tension with independent observational efforts to determine the local star formation history. While Color–Magnitude diagram inversions from Hipparcos have suggested a similarly short timescale variation in star formation of ~ 0.5 Gyr (Hernandez et al., 2000), other studies find slower variations over several Gyr (e.g. Cignoni et al., 2006). Using white dwarf cooling models to infer the local formation history (“cosmochronology”) also supports higher star formation several Gyr ago, but can rarely achieve age resolution better than ~ 1 Gyr due to small sample sizes (Tremblay et al., 2014). The spatial extent of such coherent and localized variations in star formation history is unknown.

The second scenario to explain this feature is that the period bimodality occurs due to a previously unknown variation in the spin-down evolution for low-mass stars. In this model the star formation history would be continuous over the past ~ 1 Gyr, and around 600 Myr stars would move quickly through the observed period minima due to this unknown phase

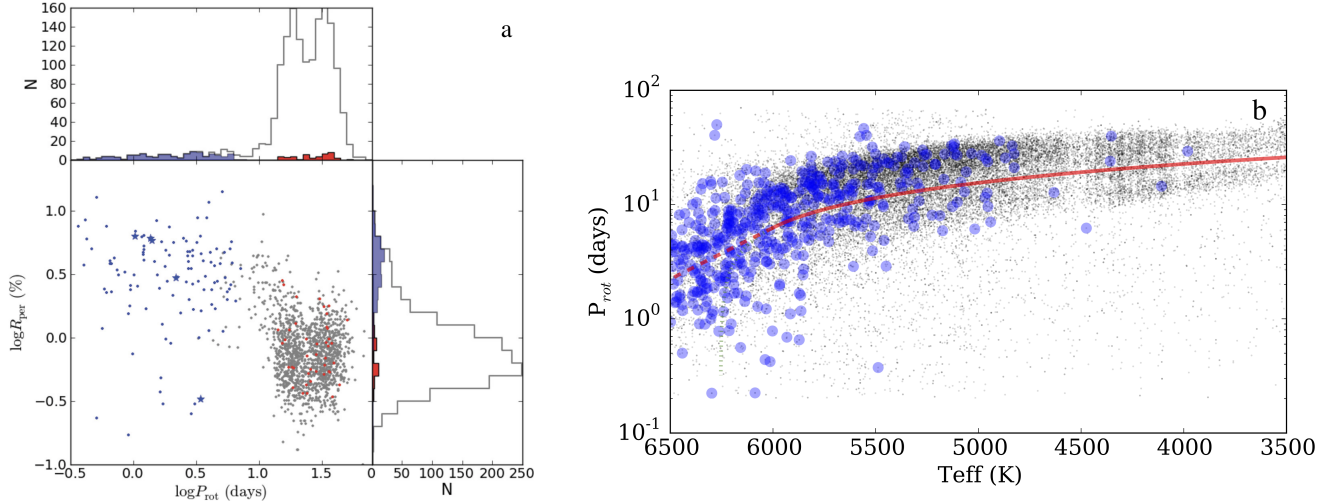


Figure 2: Left – Figure 9 from McQuillan et al. (2013); the discovery of a bimodality in rotation periods from *Kepler* M dwarfs (middle panel). Right – Figure 3 from Davenport (2017), showing all *Kepler* rotation periods from McQuillan et al. (2014) (black dots), and main sequence stars with Gaia DR1 distances (blue circles). The bimodality discovered for M dwarfs extends to nearby G and K stars, and straddles a 600 Myr “gyrochrone” (red line).

transition or feedback mechanism. While this model is not predicted by angular momentum loss prescriptions, rapid transitions in rotation period are observed for stars in young clusters. Stars move quickly from the rapidly rotating “convective” sequence (periods of $\lesssim 1$ day) to the “interface” sequence (periods of several days) during the first few hundred Myr, with lower mass stars taking longer to make this transition as they settle onto the main sequence (Barnes, 2003). Secondly, a gap in chromospheric activity levels for solar-type field stars has also been observed (Vaughan & Preston, 1980). While this magnetic activity indicator smoothly varies with stellar ages over long timescales, the gap indicates a rapid transition phase from “active” to “inactive” is present within the first Gyr (Pace et al., 2009). Thirdly, the angular momentum loss underpinning gyrochronology seems to slow for stars older than the Sun, indicating a potential change in the magnetic dynamo for slower rotators (Angus et al., 2015; van Saders et al., 2016).

The K2 rotation period sample provides the ideal dataset to test these two formation scenarios. If the bimodality is due to an age distribution we would expect to only see the feature locally, and that it could disappear at further distances or along different lines of sight where small scale variations in the star formation history are less apparent. Coherent changes in the rotation period (or stellar age) distribution along opposing Galactic lines of sight might also reveal details of the spiral arm pattern speed near the Sun. The kinematic separation between the two rotation period populations would be reinforced by supplemental measurements from the upcoming public Gaia data releases. However, if the bimodality is truly due to a transition point in the spin-down evolution at young ages, we would expect to find no little to no variation in this feature as seen in Figure 2b with galactic

position, distance, or between K2 fields.

3 Proposed Research

3.1 Measuring Rotation periods

We propose the first systematic study of stellar rotation periods from the K2 data. This will include the nearly 300,000 light curves from Campaigns 0-14.

Part of our study will be to assess the qualities of the various data reduction pipelines available for K2 light curves. Each detrending algorithm uses a slightly different approach and will almost certainly provide light curves that differ enough to produce a number of discrepant rotation periods. We will compare the performance of three pipelines in particular: the Vanderburg et al. (2015) light curves, the **everest** Luger et al. (2016) light curves, and the **K2SC** Aigrain et al. (2016) light curves. By visually examining the light curves and Lomb-Scargle periodograms of a number of targets in common between the detrending methods, we will ascertain which pipeline best preserves signal on long timescales.

Once establishing the best detrending method for preserving stellar variability, we will download all the available light curves and, if necessary, run the pipeline on any outstanding targets. We will also produce and examine periodograms using the systematics-insensitive periodogram (SIP) (Angus et al., 2015). This method simultaneously fits light curves with a sinusoid and a noise model constructed from 150 principle components derived from a PCA of the entire set of K2 light curves for a given campaign. Although developed for asteroseismology, this algorithm may also be applicable to rotation period analysis, however at the longer timescales of variation produced by stellar rotation, it is likely that the results will suffer from overfitting and will revert to standard Lomb-Scargle periodogram methods in this case.

We will use a combination of Lomb-Scargle and autocorrelation function techniques to produce a quick catalogue for early analysis. Although both of these methods are sensitive to noise and can produce spurious rotation period measurements, their relative speed will allow us to rapidly begin initial analysis of the results. We will then apply a procedure for obtaining more accurate and precise rotation periods using probabilistic inference. Co-I Angus recently developed a method for rotation period inference using a Gaussian Process (GP) to model the light curve in the time-domain, rather than extracting periodic signals in the frequency domain Angus et al. (2016a). This GP method produces slightly more precise and accurate rotation periods with more representative uncertainties than Lomb-Scargle and autocorrelation methods. The disadvantage of this GP regression based method is that it can be computationally expensive. However, with the recently developed method for fast Gaussian process inference, **celerite** (Foreman-Mackey et al., 2017), even performing MCMC with the thousands of data points in a K2 light curve may only take a few minutes. The advantage of computing probabilistic rotation periods is that one can bypass the need to calculate a rotation period at all and simply infer the parameters of stellar populations directly from the light curves themselves. In other words, one can perform hierarchical

inference more easily. This may be a level of sophistication that is above and beyond our science goals but it is worth noting that we could take this approach if the data and scientific question warranted it.

Wherever possible we will mask out discontinuous astrophysical signals, such as eclipsing binaries, planet transit or flares that may distort the rotation period signal. We will make use of exoplanet and binary catalogs to identify planet transits and eclipses. We will apply the flare detection algorithm `appaloosa`, built by PI Davenport, to identify and remove flares. It may still be necessary to apply a low-pass filter to the data in order to remove high frequency features that we miss. Fortunately, most of the stellar rotation signals of interest for this study have timescales longer than around a day and will be relatively unaffected by a low-pass filtering algorithm.

From our sample of nearly 300,000 available K2 targets, we expect to recover over 70,000 new periods, bringing the total *Kepler*/K2 sample to $\sim 100,000$ stars with measured rotation periods.

We have already measured a number of K2 rotation periods using a simple autocorrelation function approach. Figure 3 shows stars observed by K2 during campaign 4, plotted according to their RA and dec and colored by their rotation period. To measure the rotation periods shown here we downloaded a `everest` (Luger et al., 2016) light curve for every star and computed an autocorrelation function (ACF) of each light curve. We smoothed the ACFs and adopted the lag of the highest peak as the dominant period in the time series. Due to the simplicity of the period extraction technique and the fact that we have taken each period measurement at face value with no attempt to remove astrophysical contaminants, figure 3 is a *very* preliminary look at rotation and other stellar variability in one of the K2 fields.

3.2 Exploring the Period Bimodality

To determine which formation mechanism gives rise to the bimodal period distribution seen in the original *Kepler* field, we must determine if the feature is only present in nearby stars. However, we must also rule out the unlikely possibility that the bimodality is due to some systematic error in the *Kepler* data. Within each K2 campaign we will visually inspect the low-mass stars in the color-period space ($T_{eff} < 4500$), as illustrated in Figure 2 for the McQuillan et al. (2013) M dwarf sample. Since these coolest stars are only visible with *Kepler* out to a few hundred pc, this will provide a test of the localization of the bimodality, using a small volume-limited sample. This test provides an important reality check against the period bimodality being due to the processing of the original *Kepler* data itself. Since this initial nearby sample will probe the same close (~ 250 pc) volume as in McQuillan et al. (2013) and Davenport (2017), we expect the period bimodality will appear up in most K2 fields for the M dwarfs centered around $P_{rot} = 20$ days.

To reliably map the rotation period distribution as a function of distance we will match our final sample of K2 stars, and the original *Kepler* rotation sample, to the upcoming data release from the Gaia mission (Perryman et al., 2001). With accurate parallaxes from Gaia for all *Kepler* and K2 sources we will also be able to filter out

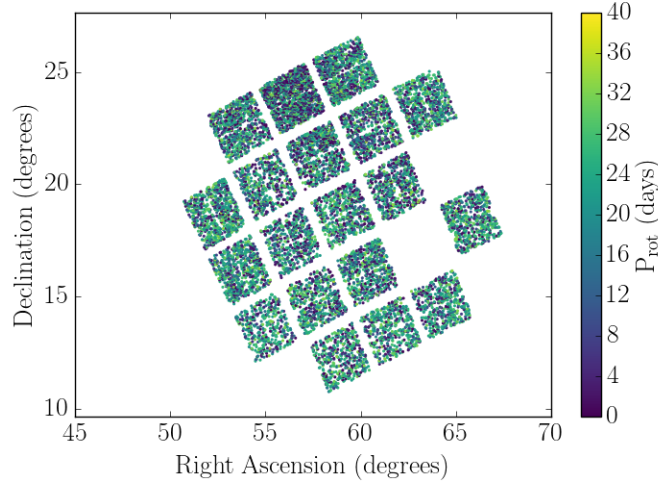


Figure 3: All stars observed during K2 campaign 4, plotted according to their equatorial coordinates and colored by their preliminary rotation period. These rotation periods were measured using a very simple ACF method, applied to *everest* (Luger et al., 2015) light curves.

subgiants and binary stars from our sample, leaving only main sequence stars. As Davenport (2017) showed, G dwarfs can only be used to detect the period bimodality if subgiants and binaries are filtered out. Davenport (2017) was able to do this for the *Kepler* rotation period sample using the Gaia DR1 “TGAS” release that included astrometric data for nearby stars (Lindgren et al., 2016), as shown in Figure 4. This reduced the McQuillan et al. (2014) rotation period sample of 33,000 sources down to the 440 brightest main sequence stars within ~ 300 pc, roughly the same distance limit reached by the M dwarf-only sample. Studying the period distribution for G dwarfs is critical for including stars at further distances, and therefore sampling different star formation histories. **With the April 2018 data release from Gaia we will be able to study rotation periods for G dwarfs in *Kepler* and K2 out to ~ 3 kpc.**

Since the K2 campaign fields are spread across the entire ecliptic plane, rotation period data from fields with similar galactic latitudes can be combined to improve the sample size when searching for the bimodality as a function of distance. For example, C1, C3, C10, and C12 are near the North and South Galactic Caps, while C2, C7, and C13 straddle the Galactic Plane. The size scale over which the Milky Way’s star formation history varies is unknown. In Andromeda significant variations in star formation histories are seen between 100 pc volumes, as well as large galaxy-wide trends (e.g. Lewis et al., 2015). We will therefore conduct our search for the period bimodality as a function of distance in each *Kepler*/K2 pointing separately, as well in bins of galactic latitude.

The variation between K2 fields in the rotation period distribution will be most sensitive

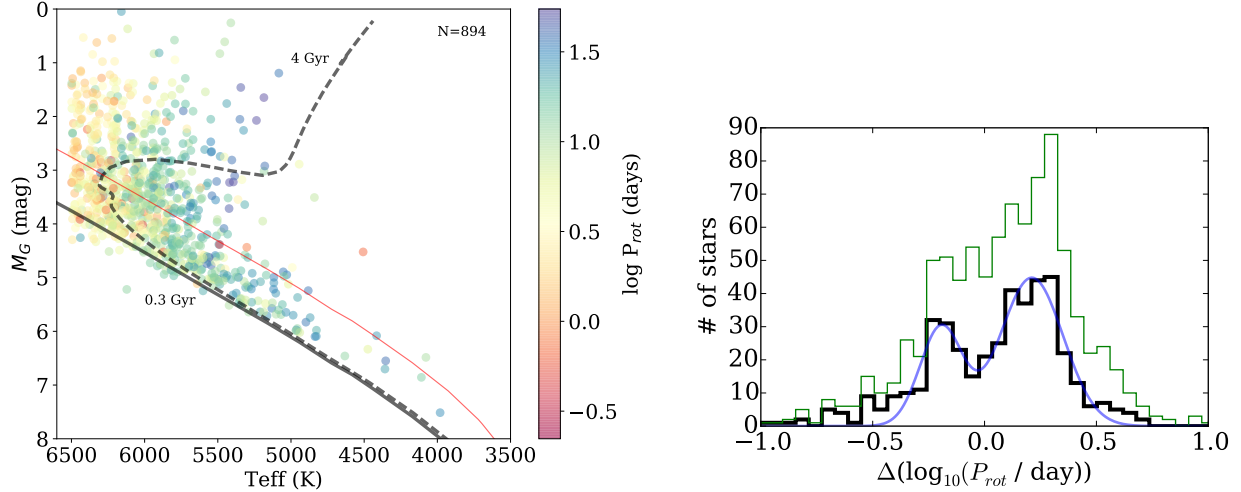


Figure 4: Left – Figure 2 from Davenport (2017), showing the absolute Gaia magnitude versus temperature for *Kepler* stars with known rotation periods in the Gaia DR1 catalog. Sub-giant stars can be separated from main sequence targets using isochrone models (black solid & dashed lines). Right – Figure 4 from Davenport (2017), showing the rotation period distribution relative to a 600 Myr “gyrochrone” before (green line) and after (black line) filtering out sub-giants. The bimodal distribution is apparent, and fit with a 2-Gaussian model (blue line).

for the youngest stars, where stellar rotation evolution is most dramatic. If the young stars (short period bump in Figure 4) were formed, for example, due to the passage of a Milky Way spiral arm, we would expect a shift in the peak of the rapid rotation distribution between fields ahead and behind the Sun along the direction of our Galactic orbit. Assuming a spiral arm pattern speed of $\Omega_{\text{sp}} = 25 \text{ km s}^{-1} \text{ kpc}^{-1}$ (Dias & Lépine, 2005; Gerhard, 2011), rapidly rotating stars at a distance of 1 kpc in opposing fields could have an age offset of ~ 100 Myr, which should be detectable given a 10-20% per-star age resolution for gyrochronology.

We will measure the strength of the bimodal feature by examining the period distribution centered around a 600 Myr gyrochrone, as in Figure 4. By fitting multiple Gaussians to the period distribution in each bin of galactic latitude and distance, we can empirically determine the significance of the bimodality. The Bayesian Information Criterion allows us to analytically determine if one or two (or more) Gaussian curves best represent the rotation distribution in each spatial bin. If the bimodality is a generic feature of angular momentum loss evolution, this two-Gaussian fit from Davenport (2017) will be preferred for every latitude and distance bin. If the bimodality is due to a localized age distribution of stars, we expect the feature will disappear or shift as we go to further distances and sample different star formation histories.

3.3 Mapping Ages in each Field

Combining our catalog of rotation periods from K2 with the existing rotation catalogs from Kepler will produce the largest set of rotation periods currently available. Using a new technique being developed by CoI Angus, **chronometer**, we will produce an improved age estimate for every star based on rotation values, photometric colors and galactic kinematics from Gaia proper motions. This age map may be used to infer the age distribution of stars within and across K2 fields.

chronometer extends isochrone fitting by simultaneously fitting an age-rotation relation and a age-velocity dispersion relation to stars with photometric colors, rotation periods and Gaia proper motions. It combines the information available from these three dating techniques, thus providing more accurate ages than any one of the techniques alone.

The accuracy of ages calculated with **chronometer** still relies on the rotational and kinematic age relations being correct. As discussed above, the performance of the age-rotation relations for old stars has been called into question in the last few years (Angus et al., 2015; van Saders et al., 2016; Metcalfe et al., 2016). A simple straight-line model for rotational age does not reproduce the ages predicted by asteroseismology for stars older than the Sun. This phenomenon is attributed to a transitioning magnetic dynamo at a critical Rossby number, Ro , of 2.6, the solar value (van Saders et al., 2016). As rotation periods slow, Ro decreases until it hits the critical value and magnetic braking switches off: stars maintain their rotation period from that point onward. This restricts the applicability of gyrochronology to young, rapidly rotating stars. This hypothesis is supported by the existing data, however these data are sparse — the analyses demonstrating the discrepancies were conducted on the small number of main sequence, Solar-like oscillators observed by Kepler in short cadence mode with detectable rotation periods: a sample size of around 20 **Ruth - check this number**. A larger sample of old main sequence stars with precise ages is required to confirm and further characterize the Rossby saturation mechanism introduced by (van Saders et al., 2016) which is currently supported by the Kepler data. However, old main sequence stars are difficult to age-date with any other method than asteroseismology. We propose use the age gradients in the kinematic properties of stars to confirm the Rossby saturation effect.

The age-velocity dispersion relations are relatively well studied and based on simple physics. There is evidence to suggest that stars in the Milky Way form in the thin disc of the galaxy with relatively small vertical velocities and angular momenta **add citations**. As time passes these stars are scattered via close encounters with other stars and interactions with galactic spiral arms. The more time passes, the more scattering events, and stars slowly accumulate angular momentum in the vertical direction, known as vertical action. This results in a slow heating of stellar orbits. Older stars can be identified in Gaia DR1 by integrating their orbits in the potential of the Milky Way to convert their proper motions, positions and parallaxes into vertical actions. It is the *dispersion* in vertical action that truly traces age, far better than vertical action itself. However for single stars only the individual's vertical action is available. Nonetheless, J_z^2 increases over time for any given star, and is a weak tracer of age. When studying populations of stars, the vertical action dispersion can be used to infer their age relatively precisely (to within 2 Gyr **Ruth, check this**). However

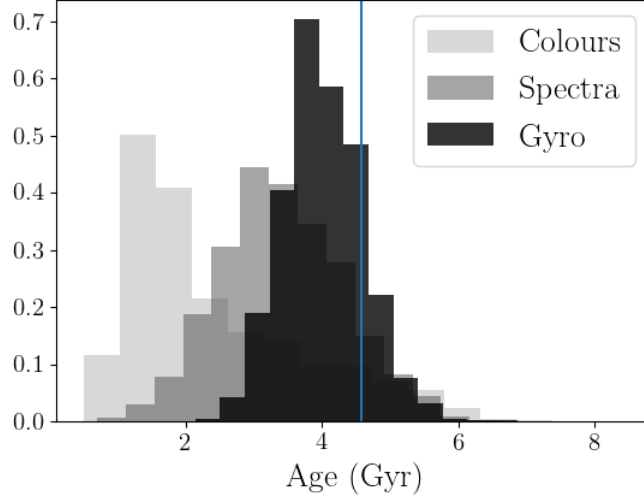


Figure 5: A preliminary demonstration of the power of rotation for age inference, created using `chronometer`. The palest gray histogram shows the probability distribution over ages obtained for the Sun at 10 parsecs using only J, H and K band colors. The darker gray histogram shows the age posterior for the Sun at 10 parsecs using colors and spectroscopic information (T_{eff} , $\log(g)$ and $[Fe/H]$). The darkest gray histogram shows the age posterior when colors, spectroscopic information and a rotation period used to infer the age of the Sun at 10 parsecs. This is a preliminary plot with no kinematic information and just three stars. The final model will contain several thousand stars and kinematic information so will be even more powerful than this.

for single stars vertical action can only constrain ages to within 4 Gyr.

A simple test will allow us to distinguish between two magnetic braking scenarios in MS stars: the continuous scenario in which stars begin magnetic braking at zero-age main sequence and continue until main sequence turn off, and the transition scenario in which stars stop braking at a critical Rossby number. This test involves computing rotation-based ages for stars observed by both Kepler and Gaia. Each star will have ages computed using the continuous scenario and the transition scenario. The vertical action dispersion will then be calculated for groups of stars with similar rotational age, producing two vertical action-age relations. The vertical action dispersion will also be calculated for red giants observed by APOGEE with ages from the Cannon (Ness et al., 2015), observed by Gaia. This red giant vertical action-age relation will serve as our "ground truth" since these ages are relatively robust and well calibrated with asteroseismic giants. We will compare the both the σ_{J_z} -age relation for the continuous scenario and the σ_{J_z} -age relation for the transition scenario with the red giant σ_{J_z} -age relation. This test will reveal whether continuous magnetic braking or transitional magnetic braking provides a better description of the data.

This test will allow us to select an appropriate age rotation relation to be used in

chronometer, our new age-dating method for MS stars. **chronometer** combines the following dating methods: gyrochronology, isochrone fitting, asteroseismology and galactic kinematics into one model by jointly inferring the parameters of the three different models. In classical isochrone fitting, one might calculate the probability of age A , mass M , $[Fe/H]$, distance D and extinction A_v , given a set of apparent magnitudes in different filters, *e.g.* M_V , M_J and M_K . There are no free parameters in the model here — the model is entirely determined by physics and does not need to be calibrated further. A suitable set of stellar evolution models would be selected for the inference, for example the Dartmouth models **Ruth: add citation**. Similarly, in classical gyrochronology, one might calculate the probability of age given rotation period and $B - V$ colour, In a gyrochronology model however, our understanding of the physics is incomplete and some free parameters must be calibrated. In the Barnes (2003) gyrochronology parameterisation, $A = P_{\text{rot}}^{1/n} - (B - V - 0.4)^{b/n}$, these free parameters are a , b and n . During a calibration exercise, the observables, A , P_{rot} and $B - V$ will be known and the parameters, a , b and n will be inferred. The age-velocity dispersion relation also has free parameters that must be calibrated using observations, for example the coefficient of increasing dispersion.

The unique aspect of our analysis is to combine inference over ages with calibration of the free parameters in the gyrochronology and vertical action-age relations. The global parameters, the parameters of the gyrochronology relation and the age-velocity dispersion relation will be inferred separately from the individual parameters of each star. This inference problem involves a lot of free parameters: at least four global parameters and five parameters per star. Inferring the ages of one thousand stars will require sampling the posterior probability density functions of five thousand and four parameters. This sounds like a large number but we can use conditional independence to break this problem down and apply Gibbs sampling to increase tractability. This means we will only explore the PDFs of a maximum of five parameters at a time. Informally, the structure of this inference procedure can be written as

$$\begin{aligned}
 & p(\text{Ages \& other parameters} | \text{observables}) & (1) \\
 \propto & \mathcal{L}_{\text{isochronal age}} \times \mathcal{L}_{\text{gyro age}} \times \mathcal{L}_{\text{kinematic age}} & (2) \\
 & \times p(\text{Ages \& other parameters}) & (3)
 \end{aligned}$$

This is essentially an extension of the period bimodality work (if it's an age effect), but to create a detailed map of the ages of these field stars at a range of galactic latitudes in the 17 pencil-beams available from K2. combining with the periods from Kepler, will be even better. Ultimately we'd like to compare to the age distributions in simulations of these fields from TRILEGAL, and from other age indicators (asteroseismology, flare ages, etc).

4 Team Qualifications

PI Davenport has used *Kepler* to conduct the largest survey to-date of stellar activity from flares, as well as multiple investigations of starspots and their evolution with time using

Kepler data. From these studies, Davenport has developed an age model for flare activity that will be directly comparable to the ages and starspot amplitudes derived from this study. He also recently discovered the rotation period bimodality first noted with *Kepler* M dwarfs by McQuillan et al. (2013) extends to G and K dwarf stars (Davenport, 2017). Davenport previously collaborated on NASA ADP grant NNX09AC77G to characterize NIR variability using the 2MASS Calibration Scan Point Source Working Database (Davenport et al., 2012, 2015). He has mentored numerous students on projects using *Kepler* data, resulting in student-led publications such as the flare activity of a unique M dwarf binary system GJ 1245AB (Lurie et al., 2015), and exploring the poorly understood origins of wide binary stars through stellar rotation (R. Clarke in prep). He will manage the overall project, detect and remove short period variability from flares in the light curves, supervise the initial periodic signal detection using Lomb-Scargle methods, and lead the investigation and publication on the nature of the bimodal period distribution.

Co-I Angus is an expert in the extraction of periodic signals from *Kepler* data using Gaussian Processes (Angus et al., 2016a) and other cutting-edge statistical techniques. She is the author of tools for generating Systematics-Insensitive Periodograms for both *Kepler* and K2 data (Angus et al., 2016b), as well as new gyrochronology calibrations using *Kepler* asteroseismic targets (Angus et al., 2015). She will lead the effort to measure and publish the catalog of rotation periods for all K2 sources, and guide students in measuring ages for field stars using the `chronometer` Python code.

Covey wrote white paper of stellar age dating techniques for decadal survey (Covey et al., 2009) expertise working with *Kepler* and K2 data to search for periods (Douglas et al., 2016; Covey et al., 2016)

Kipping has developed analytical models for rotational modulations in stellar light curves (Kipping, 2012), and recently used Gaussian Processes to detrend systematics and search for periodicities from MOST data of Proxima Centauri (Kipping & et al., 2016). He will provide expertise in advanced statistical techniques to detrend and study the K2 data to help Co-I Angus in her period detection and validation efforts.

Agueros ongoing study of rotation in clusters from both the ground (Agüeros et al., 2011) and with *Kepler*/K2 Douglas et al. (2016, 2017); Núñez et al. (2017).

5 Relevance to NASA Programs

history of MWY, age of planet systems, TESS

6 Plan of Work

Year 1: process all rotation period data

Year 2: write papers

References

- Agüeros, M. A., Covey, K. R., Lemonias, J. J., et al. 2011, *ApJ*, 740, 110
- Aigrain, S., Parviainen, H., & Pope, B. J. S. 2016, *MNRAS*, 459, 2408
- Aigrain, S., Llama, J., Ceillier, T., et al. 2015, *MNRAS*, 450, 3211
- Angus, R., Aigrain, S., & Foreman-Mackey, D. 2016a, *IAU Focus Meeting*, 29, 191
- Angus, R., Aigrain, S., Foreman-Mackey, D., & McQuillan, A. 2015, *MNRAS*, 450, 1787
- Angus, R., Foreman-Mackey, D., & Johnson, J. A. 2016b, *ApJ*, 818, 109
- Barnes, S. A. 2003, *ApJ*, 586, 464
- . 2007, *ApJ*, 669, 1167
- . 2010, *ApJ*, 722, 222
- Borucki, W. J., Koch, D., Basri, G., et al. 2010, *Science*, 327, 977
- Charbonneau, P. 2010, *Living Reviews in Solar Physics*, 7, doi:10.12942/lrsp-2010-3
- Cignoni, M., Degl’Innocenti, S., Prada Moroni, P. G., & Shore, S. N. 2006, *A&A*, 459, 783
- Collins, II, G. W., & Truax, R. J. 1995, *ApJ*, 439, 860
- Covey, K. R., Beers, T. C., Bochanski, J. J., et al. 2009, in *ArXiv Astrophysics e-prints*, Vol. 2010, *astro2010: The Astronomy and Astrophysics Decadal Survey*, 57
- Covey, K. R., Agüeros, M. A., Law, N. M., et al. 2016, *ApJ*, 822, 81
- Davenport, J. R. A. 2017, *ApJ*, 835, 16
- Davenport, J. R. A., Becker, A. C., Kowalski, A. F., et al. 2012, *ApJ*, 748, 58
- Davenport, J. R. A., Ruan, J. J., Becker, A. C., Macleod, C. L., & Cutri, R. M. 2015, *ApJ*, 803, 2
- Dias, W. S., & Lépine, J. R. D. 2005, *ApJ*, 629, 825
- Douglas, S. T., Agüeros, M. A., Covey, K. R., et al. 2016, *ApJ*, 822, 47
- Douglas, S. T., Agüeros, M. A., Covey, K. R., & Kraus, A. L. 2017, *ArXiv e-prints*, arXiv:1704.04507
- Douglas, S. T., Agüeros, M. A., Covey, K. R., et al. 2014, *ApJ*, 795, 161

- Foreman-Mackey, D., Agol, E., Angus, R., & Ambikasaran, S. 2017, ArXiv e-prints, arXiv:1703.09710
- Gerhard, O. 2011, *Memorie della Societa Astronomica Italiana Supplementi*, 18, 185
- Hartman, J. D., Bakos, G. Á., Noyes, R. W., et al. 2011, *AJ*, 141, 166
- Hayden, M. R., Holtzman, J. A., Bovy, J., et al. 2014, *AJ*, 147, 116
- Hernandez, X., Valls-Gabaud, D., & Gilmore, G. 2000, *MNRAS*, 316, 605
- Howell, S. B., Sobeck, C., Haas, M., et al. 2014, *PASP*, 126, 398
- Irwin, J., & Bouvier, J. 2009, in *IAU Symposium*, Vol. 258, *The Ages of Stars*, ed. E. E. Mamajek, D. R. Soderblom, & R. F. G. Wyse, 363–374
- Kawaler, S. D. 1988, *ApJ*, 333, 236
- Kipping, D. M. 2012, *MNRAS*, 427, 2487
- Kipping, D. M., & et al. 2016, *ApJ*
- Lewis, A. R., Dolphin, A. E., Dalcanton, J. J., et al. 2015, *ApJ*, 805, 183
- Lindgren, L., Lammers, U., Bastian, U., et al. 2016, *A&A*, 595, A4
- Luger, R., Agol, E., Kruse, E., et al. 2016, *AJ*, 152, 100
- Luger, R., Barnes, R., Lopez, E., et al. 2015, *Astrobiology*, 15, 57
- Lurie, J. C., Davenport, J. R. A., Hawley, S. L., et al. 2015, *ApJ*, 800, 95
- Mamajek, E. E., & Hillenbrand, L. A. 2008, *ApJ*, 687, 1264
- Matt, S. P., MacGregor, K. B., Pinsonneault, M. H., & Greene, T. P. 2012, *ApJ*, 754, L26
- McQuillan, A., Aigrain, S., & Mazeh, T. 2013, *MNRAS*, 432, 1203
- McQuillan, A., Mazeh, T., & Aigrain, S. 2014, *ApJS*, 211, 24
- Mestel, L. 1984, in *Lecture Notes in Physics*, Berlin Springer Verlag, Vol. 193, *Cool Stars, Stellar Systems, and the Sun*, ed. S. L. Baliunas & L. Hartmann, 49
- Metcalfe, T. S., Egeland, R., & van Saders, J. 2016, *ApJ*, 826, L2
- Ness, M., Hogg, D. W., Rix, H.-W., Ho, A. Y. Q., & Zasowski, G. 2015, *ApJ*, 808, 16
- Noyes, R. W., Hartmann, L. W., Baliunas, S. L., Duncan, D. K., & Vaughan, A. H. 1984, *ApJ*, 279, 763

- Núñez, A., Agüeros, M. A., Covey, K. R., & López-Morales, M. 2017, *ApJ*, 834, 176
- Pace, G., Melendez, J., Pasquini, L., et al. 2009, *A&A*, 499, L9
- Parker, E. N. 1970, *ApJ*, 162, 665
- Perryman, M. A. C., de Boer, K. S., Gilmore, G., et al. 2001, *A&A*, 369, 339
- Radick, R. R., Thompson, D. T., Lockwood, G. W., Duncan, D. K., & Baggett, W. E. 1987, *ApJ*, 321, 459
- Reinhold, T., Reiners, A., & Basri, G. 2013, *A&A*, 560, A4
- Schatzman, E. 1962, *Annales d'Astrophysique*, 25, 18
- Skumanich, A. 1972, *ApJ*, 171, 565
- Tremblay, P.-E., Kalirai, J. S., Soderblom, D. R., Cignoni, M., & Cummings, J. 2014, *ApJ*, 791, 92
- van Saders, J. L., Ceillier, T., Metcalfe, T. S., et al. 2016, *Nature*, 529, 181
- van Saders, J. L., & Pinsonneault, M. H. 2013, *ApJ*, 776, 67
- Vanderburg, A., Johnson, J. A., Rappaport, S., et al. 2015, *Nature*, 526, 546
- Vaughan, A. H., & Preston, G. W. 1980, *PASP*, 92, 385
- Weber, E. J., & Davis, Jr., L. 1967, *ApJ*, 148, 217